

Optically generated reconfigurable photonic structures of elastic quasiparticles in frustrated cholesteric liquid crystals

Ivan I. Smalyukh,^{1,2,3,4,*} Daniel Kaputa,² Aliaksandr V. Kachynski,² Andrey N. Kuzmin,² Paul J. Ackerman,^{1,3} Christopher W. Twombly,¹ Taewoo Lee,¹ Rahul P. Trivedi,^{1,3} and Paras N. Prasad^{2,5}

¹Department of Physics and Liquid Crystal Materials Research Center, University of Colorado, Boulder, Colorado 80309, USA

²The Institute for Lasers, Photonics, and Biophotonics, University at Buffalo, The State University of New York, Buffalo, New York 14260, USA

³Department of Electrical, Computer, and Energy Engineering and Materials Science Engineering Program, University of Colorado, Boulder, Colorado 80309, USA

⁴Renewable and Sustainable Energy Institute, National Renewable Energy Laboratory and University of Colorado, Boulder, Colorado 80309, USA

⁵pnprasad@buffalo.edu

*ivan.smalyukh@colorado.edu

Abstract: We describe laser-induced two-dimensional periodic photonic structures formed by localized particle-like excitations in an untwisted confined cholesteric liquid crystal. The individual particle-like excitations (dubbed “Torons”) contain three-dimensional twist of the liquid crystal director matched to the uniform background director field by topological point defects. Using both single-beam-steering and holographic pattern generation approaches, the periodic crystal lattices are tailored by tuning their periodicity, reorienting their crystallographic axes, and introducing defects. Moreover, these lattices can be dynamically reconfigurable: generated, modified, erased and then recreated, depending on the needs of a particular photonic application. This robust control is performed by tightly focused laser beams of power 10-100 mW and by low-frequency electric fields at voltages ~10 V applied to the transparent electrodes.

© 2012 Optical Society of America

OCIS codes: (160.3710) Liquid crystals; (140.7010) Laser trapping; (050.5298) Photonic crystals; (190.0190) Nonlinear optics; (180.6900) Three-dimensional microscopy.

References and links

1. J. D. Joannopoulos, S. G. Johnson, J. N. Winn, and R. D. Meade, *Photonic Crystals: Molding the Flow of Light*, 2nd ed. (Princeton Univ. Press, 2008).
2. K. Busch, G. von Freymann, S. Linden, S. F. Mingaleev, L. Tkeshelashvili, and M. Wegener, “Periodic nanostructures for photonics,” *Phys. Rep.* **444**(3-6), 101–202 (2007).
3. E. Yablonovitch, “Inhibited spontaneous emission in solid-state physics and electronics,” *Phys. Rev. Lett.* **58**(20), 2059–2062 (1987).
4. S. John, “Strong localization of photons in certain disordered dielectric superlattices,” *Phys. Rev. Lett.* **58**(23), 2486–2489 (1987).
5. J. Yamamoto and H. Tanaka, “Dynamic control of the photonic smectic order of membranes,” *Nat. Mater.* **4**(1), 75–80 (2005).
6. H. J. Coles and M. N. Pivnenko, “Liquid crystal ‘blue phases’ with a wide temperature range,” *Nature* **436**(7053), 997–1000 (2005).
7. P. N. Prasad, *Nanophotonics* (John Wiley & Sons, Inc. 2004).
8. B. Y. Zhang, F. B. Meng, and Y. H. Cong, “Optical characterization of polymer liquid crystal cell exhibiting polymer blue phases,” *Opt. Express* **15**(16), 10175–10181 (2007).
9. S. J. Woltman, G. D. Jay, and G. P. Crawford, “Liquid-crystal materials find a new order in biomedical applications,” *Nat. Mater.* **6**(12), 929–938 (2007).
10. P.-G. de Gennes and J. Prost, *The Physics of Liquid Crystals*, 2nd ed. (Clarendon, 1993).
11. P. M. Chaikin and T. C. Lubensky, *Principles of Condensed Matter Physics* (Cambridge University Press, 1995).

12. I. I. Smalyukh, B. I. Senyuk, P. Palffy-Muhoray, O. D. Lavrentovich, H. Huang, E. C. Gartland, Jr., V. H. Bodnar, T. Kosa, and B. Taheri, "Electric-field-induced nematic-cholesteric transition and three-dimensional director structures in homeotropic cells," *Phys. Rev. E Stat. Nonlin. Soft Matter Phys.* **72**(6), 061707 (2005).
13. P. Oswald, J. Baudry, and S. Pirkel, "Static and dynamic properties of cholesteric fingers in electric field," *Phys. Rep.* **337**(1-2), 67–96 (2000).
14. I. I. Smalyukh, Y. Lansac, N. A. Clark, and R. P. Trivedi, "Three-dimensional structure and multistable optical switching of triple-twisted particle-like excitations in anisotropic fluids," *Nat. Mater.* **9**, 139–145 (2010).
15. E. Brasselet, N. Murazawa, H. Misawa, and S. Juodkazis, "Optical vortices from liquid crystal droplets," *Phys. Rev. Lett.* **103**(10), 103903 (2009).
16. O. Trushkevych, P. Ackerman, W. A. Crossland, and I. I. Smalyukh, "Optically generated adaptive localized structures in confined Chiral liquid crystals doped with fullerene," *Appl. Phys. Lett.* **97**(20), 201906 (2010).
17. D. Engström, R. P. Trivedi, M. Persson, M. Goksör, K. A. Bertness, and I. I. Smalyukh, "Three-dimensional imaging of liquid crystal structures and defects by means of holographic manipulation of colloidal nanowires with faceted sidewalls," *Soft Matter* **7**(13), 6304–6312 (2011).
18. I. I. Smalyukh, A. V. Kachynski, A. N. Kuzmin, and P. N. Prasad, "Laser trapping in anisotropic fluids and polarization-controlled particle dynamics," *Proc. Natl. Acad. Sci. U.S.A.* **103**(48), 18048–18053 (2006).
19. R. P. Trivedi, D. Engström, and I. I. Smalyukh, "Optical manipulation of colloids and defect structures in anisotropic liquid crystal fluids," *J. Opt.* **13**(4), 044001 (2011).
20. T. Lee, R. P. Trivedi, and I. I. Smalyukh, "Multimodal nonlinear optical polarizing microscopy of long-range molecular order in liquid crystals," *Opt. Lett.* **35**(20), 3447–3449 (2010).
21. A. V. Kachynski, A. N. Kuzmin, P. N. Prasad, and I. I. Smalyukh, "Coherent anti-Stokes Raman scattering polarized microscopy of three-dimensional director structures in liquid crystals," *Appl. Phys. Lett.* **91**(15), 151905 (2007).
22. R. P. Trivedi, T. Lee, K. A. Bertness, and I. I. Smalyukh, "Three dimensional optical manipulation and structural imaging of soft materials by use of laser tweezers and multimodal nonlinear microscopy," *Opt. Express* **18**(26), 27658–27669 (2010).
23. I.-C. Khoo, *Liquid Crystals: Physical Properties and Nonlinear Optical Phenomena* (Wiley, 1995).
24. S. D. Durbin, S. M. Arakelian, and Y. R. Shen, "Optical-field-induced birefringence and Freedericksz transition in a nematic liquid crystal," *Phys. Rev. Lett.* **47**(19), 1411–1414 (1981).
25. E. Santamato, G. Abbate, P. Maddalena, and Y. R. Shen, "Optically induced twist Fréedericksz transitions in planar-aligned nematic liquid crystals," *Phys. Rev. A* **36**(5), 2389–2392 (1987).
26. I. C. Khoo, T. H. Liu, and P. Y. Yan, "Nonlocal radial dependence of laser-induced molecular reorientation in a nematic liquid crystal: theory and experiment," *J. Opt. Soc. Am. B* **4**, 115 (1987).
27. V. G. Bhidé, S. Chandra, S. C. Jain, and R. K. Medhekar, "Structure and properties of bubble domains in cholesteric-nematic mixtures," *J. Appl. Phys.* **47**(1), 120–126 (1976).
28. J. Buey, L. Diez, P. Espinet, H.-S. Kitzerow, and J. A. Miguel, "Optical storage effect in a platinum orthometalated liquid crystal," *Appl. Phys. B* **66**(3), 355–358 (1998).
29. T. Akahane and T. Tako, "Molecular alignment of cholesteric bubble domains cholesteric-nematic mixtures," *Jpn. J. Appl. Phys.* **15**(8), 1559–1560 (1976).
30. S. Pirkel, P. Ribiere, and P. Oswald, "Forming process and stability of bubble domains in dielectrically positive cholesteric liquid crystals," *Liq. Cryst.* **13**(3), 413–425 (1993).
31. J. M. Gilli and L. Gil, "Static and dynamic textures obtained under an electric field in the neighborhood of the winding transition of a strongly confined cholesteric," *Liq. Cryst.* **17**(1), 1–15 (1994).
32. B. Kerllenevich and A. Coche, "Bubble domains in cholesteric liquid crystals," *Mol. Cryst. Liq. Cryst. (Phila. Pa.)* **68**(1), 47–55 (1981).
33. W. E. L. Haas and J. E. Adams, "New optical storage mode in liquid crystals," *Appl. Phys. Lett.* **25**(10), 535–537 (1974).

1. Introduction

Photonic crystals are shaping future of technologies and devices [1–4]. These materials have alternating domains with different refractive indices forming an ordered dielectric structure with the periodicity comparable to the wavelength of light. One-dimensional (1D), two-dimensional (2D), or three-dimensional (3D) periodic photonic crystal media allow light to be routed through complex circuits, resembling the electric current in electronic chips [1–4]. They have attracted a remarkable wealth of research activities fueled both by a quest for fundamental understanding of new phenomena and by their potential for technological applications [2]. Many interesting and useful properties have been observed to arise in the periodic dielectric materials even if the contrast of refractive index between the periodically alternating domains is not high enough to provide a full photonic band gap [5–9]. For example, mirror-free lasers with distributed feedback have been demonstrated using self-assembled periodic ground-state structures in cholesteric and blue phases of chiral liquid crystals (LCs) reminiscent of the 1D and 3D photonic crystals, respectively [6, 7]. However,

anticipated photonic crystal applications are often hindered because of their limited dynamic control by external fields and light [7].

We describe a robust optical and electrical control of 2D photonic lattices in chiral LCs that have twisted molecular alignment in the ground state. The axis of molecular twist in cholesteric LCs (CLCs) is called the helical axis and the spatial period over which the director $\hat{n}(\vec{r})$ (a unit vector with non-polar symmetry describing the local average molecular orientation) twists through 360° is called the cholesteric pitch p [10, 11]. CLCs can be composed of a single chemical compound with chiral molecules lacking mirror symmetry as well as of mixtures of a nematic host and one or more chiral additives [10]. The equilibrium cholesteric pitch p can be modified by varying concentration of the additive and is often within the range from 100 nm to 100 μm , thus enabling formation of periodic structures for photonic applications in ultraviolet, visible, and infrared spectral ranges. When CLCs are confined in cells with different boundary conditions or subjected to electric or magnetic fields, one often observes complex 3D structures [10–17]. The cholesteric helix can be distorted or even completely unwound by confining the material between two substrates treated to produce homeotropic boundary conditions [12–14]. Competing factors, such as chirality, elasticity, surface anchoring, and coupling to low-frequency electric field and optical-frequency electric field of the laser beam, result in a rich variety of controlled orientational structures, ranging from untwisted uniform director field to cholesteric fingers, bubbles, and periodic arrays of triple-twisted elastic quasiparticles dubbed “Torons” [12–14]. In this work, we use focused laser beams at low powers and electric fields produced by AC voltages $\sim 10\text{V}$ to induce local transitions between different structures. We demonstrate that the geometry of initially unwound CLC in a homeotropic cell of thickness comparable to the equilibrium ground-state pitch allows for a robust generation and control of 2D periodic lattices that are shown to be composed of triple twisted Toron quasiparticles of the first kind (T3-1s) [14]. We discuss the physical underpinnings of laser-induced realignment in CLCs and describe generation of desired photonic structures using both time-shared scanned beam and holographic laser generation approaches. We further show that these photonic structures can be dynamically altered by applying electric fields and voltage to make them reconfigurable.

2. Materials, sample preparation, and experimental techniques

2.1 Materials and cell preparation

Cholesteric mixtures were prepared using nematic hosts MLC-6815 and MLC-6609 and the chiral additives ZLI-811 and CB-15 (all materials purchased from EM Industries). The helical twisting power of the chiral additives in the used nematic hosts was determined using the method of Grandjean-Cano wedge [16, 17]. The low-frequency dielectric anisotropy of the MLC-6609 host is negative ($\Delta\varepsilon_{6609} = -3.7$) and that of MLC-6815 is positive ($\Delta\varepsilon_{6815} = 8.1$). The studied cells were assembled using glass plates coated with transparent ITO electrodes and the polyimide JALS-204 (purchased from JSR, Japan) as a homeotropic alignment layer. JALS-204 provides strong vertical boundary conditions for the LC director. The cell gap thickness d was set to be in the range within 5–15 μm using either the glass micro-sphere spacers uniformly distributed within the area of a cell (one spacer per $\sim 0.5\text{ mm}^2$ area) or strips of Mylar film placed along the cell edges. We constructed a series of cells of different thickness and filled them with materials of different pitch p approximately equal to d . Constant and modulated amplitude electric signals were applied to the cells using a function generator (model DS345, Stanford Research Systems) and a wide-band amplifier (model 7602, Krohn-Hite), which enabled the use of a wide range of frequencies 10–10000 Hz.

2.2 CLC structure generation and imaging

For the laser-assisted control of spatially periodic structures of Torons, we have used two different approaches. In the first one, the beam of TEM₀₀ CW Nd: YAG laser (Compass 1064, Coherent Inc.) at the wavelength $\lambda = 1064\text{ nm}$ was steered using an optical manipulator

integrated with an inverted optical microscope [18]. This steering was achieved at kHz rates by using a computer-controlled galvano-mirror pair. We have also used a holographic optical LC alignment system (HOLCAS) allowing us to generate arbitrary (including periodic) patterns of laser intensity in the sample [14, 19]. The HOLCAS system consists of a LC spatial light modulator (SLM, from Boulder Nonlinear Systems) and a continuous wave Ytterbium-doped fiber laser ($\lambda = 1064$ nm, from IPG Photonics). The 5mm laser beam diameter is first expanded to overfill the active area of the SLM and then reduced to the size of the back aperture of the microscope objective using two telescopes in the optical train, one before and another after the SLM. The SLM-modulated light is imaged at the back aperture of the microscope objective acting as a Fourier transform lens [19]. In both approaches, the laser beams were focused using immersion oil objectives $40\times$, $60\times$, and $100\times$ and air objectives $10\times$ and $20\times$. The laser power was varied within 0-120 mW.

Simultaneously with the generation of the structures, we conducted bright-field and polarized microscopy observations. Vertical cross-sections perpendicular to the plane of a cell were visualized using the three-photon excitation fluorescence polarized microscopy (3PEF-PM) that utilizes fluorescence signals from the LC molecules excited through a three-photon absorption process [20]. The advantage of using this technique is that, unlike fluorescence confocal polarizing microscopy and similar to the case of the coherent anti-Stokes Raman scattering (CARS) microscopy, the 3PEF-PM does not require doping samples with dyes (since the fluorescence signals are due to the LC molecules themselves) but provides stronger signal in polarization-sensitive textures as compared to CARS microscopy [20–22]. We reconstruct $\hat{n}(\vec{r})$ using cross-sections obtained for circular and different linear polarizations. The use of small excitation laser powers ($\ll 1$ mW) assures that laser beam scanned through the sample for imaging purposes does not alter $\hat{n}(\vec{r})$ [21, 22].

3. Theory

Laser-induced realignment of LC director is an optical-frequency version of the Freedericksz transition that forms the basis for modern display applications [23]. The threshold nature of this director realignment in the initially uniformly aligned LC cell with strong surface anchoring for the director is a result of competition between the optical and elastic torques [23–26]. The elastic free energy density describing elastic distortions in the CLC reads [10,11]:

$$f_{elastic} = \frac{K_{11}}{2} (\nabla \cdot \hat{n})^2 + \frac{K_{22}}{2} [\hat{n} \cdot (\nabla \times \hat{n}) + \frac{2\pi}{p}]^2 + \frac{K_{33}}{2} [\hat{n} \times (\nabla \times \hat{n})]^2 - K_{24} \{ \nabla \cdot [\hat{n} (\nabla \times \hat{n}) + \hat{n} \times (\nabla \times \hat{n})] \}, \quad (1)$$

where K_{11} , K_{22} , K_{33} , and K_{24} are Frank elastic constants for splay, twist, bend and saddle splay deformations, respectively. The effects of optical-frequency electric field of the laser beam as well as low-frequency AC electric field \vec{E} (when voltage is applied to cell's transparent electrodes) can be described using a free energy density term [10, 23]:

$$f_{electric} = -\frac{\epsilon_0}{2} \Delta\epsilon (\vec{E} \cdot \hat{n})^2 \quad (2)$$

where ϵ_0 is vacuum permittivity and dielectric anisotropy at low frequencies $\Delta\epsilon = \Delta\epsilon_{lf}$ contains both electronic and dipole contributions and can be positive or negative, depending on the used LC material. At optical frequencies $\Delta\epsilon = \Delta\epsilon_{of} = n_e^2 - n_o^2$, where n_e and n_o are extraordinary and ordinary refractive indices at the beam's wavelength, respectively.

In a homeotropic cell with the initial uniform alignment of unwound director shown in Fig. 1(a), a laser-induced director realignment occurs (Fig. 1(b)) when the electric torque (tending to reorient the LC director parallel to \vec{E}) overcomes the elastic torque (tending to preserve the initial uniform alignment). From the balance of elastic and electric torques

corresponding to the free energy densities given by Eq. (1) and Eq. (2), one derives the expression for the threshold of applied low-frequency AC voltage U_{th} at which the LC director starts to reorient:

$$U_{th} = \pi \sqrt{(1 - 4\rho^2 K_{22}^2 / K_{33}^2) \cdot (K_{33} / \Delta\varepsilon)} = U_{th_nematic} \sqrt{1 - 4\rho^2 K_{22}^2 / K_{33}^2}, \quad (3)$$

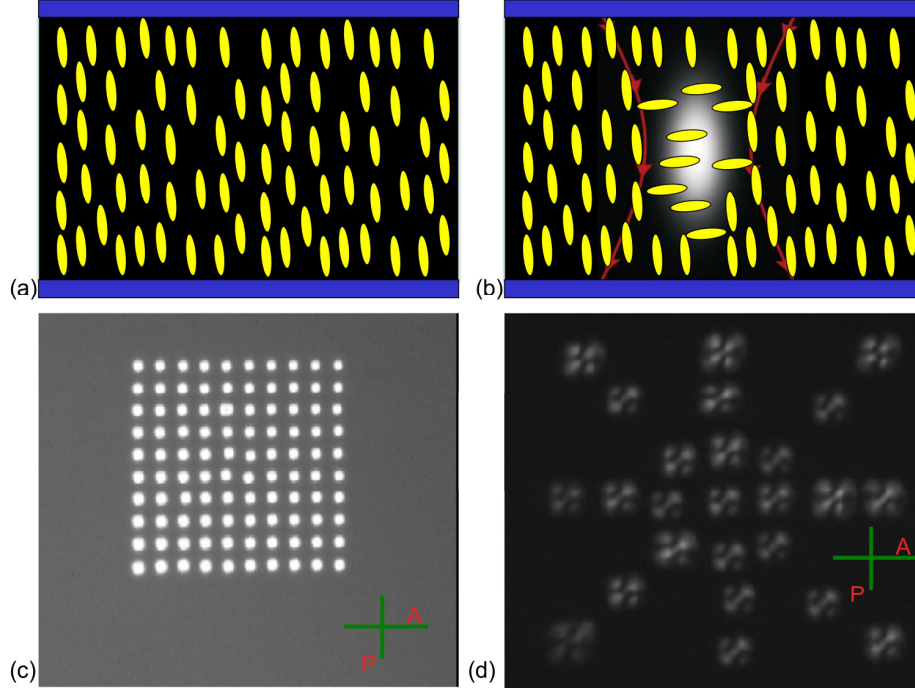


Fig. 1. Optical realignment and generation of localized structures in homeotropic CLC cells. (a,b) Schematics of (a) the initial uniform director configuration in the homeotropic unwound cholesteric and (b) the laser-induced realignment of $\hat{n}(\vec{r})$. (c) Dynamically-generated periodic structures induced using laser intensities $I_{th} < I < I_{th2}$; the distortions of $\hat{n}(\vec{r})$ are continuously induced in the new locations of an unwound cholesteric cell (Media 1) and disappear after a typical for thin cells LC relaxation time of 5-10 ms after the laser beam is shifted to a new location or switched off; the width of the image is 200 μm . (d) Polarized optical micrograph showing a 2D pattern of Torons stable after turning off the laser; the 100 μm -wide pattern is sequentially generated by using a scanned laser beam of intensity $I > I_{th2}$ (Media 2).

where the nonlocal field effects are neglected and $\rho = d/p$ is the confinement ratio of the cell thickness and the equilibrium cholesteric pitch. The threshold voltage for the untwisted cholesteric cell is lower by a factor of $(1 - 4\rho^2 K_{22}^2 / K_{33}^2)^{1/2}$ as compared to the threshold voltage $U_{th_nematic}$ for a nematic LC in the same confinement geometry.

Obtaining an analytical expression for the threshold laser intensity needed to distort $\hat{n}(\vec{r})$ is difficult due to a complex spatial distribution of the electric field of the focused Gaussian beam in the LC sample [23]. However, a number of useful physical insights and an analytical expression for rough estimates can be often obtained by introducing several simplifying assumptions [23]. Assuming that the laser beam's waist is larger than the LC cell thickness ($w > d$) and that electric field across the sample thickness is uniform (note that this assumption is reasonable only for some of the used objectives of relatively low numerical aperture < 0.5), the threshold electric field of the optical wave and corresponding laser intensity can be found similarly to the low-frequency case above. From the balance of optical and elastic torques, one finds the threshold laser beam's intensity at which the light-induced director reorientation starts in a homeotropic untwisted cholesteric LC cell:

$$I_{th} = \frac{(\pi^2 K_{33} c n_e^2)}{(n_e^2 - n_o^2) n_o d^2} \cdot (1 - 4\rho^2 \frac{K_{22}^2}{K_{33}^2}), \quad (4)$$

where c is the speed of light. The threshold intensity for the director reorientation in the frustrated CLC is smaller than in the nematic case by a factor of $(1 - 4\rho^2 K_{22}^2 / K_{33}^2)$. For $\rho = 0$, Eq. (4) reduces to the expression for the threshold realignment intensity in a homeotropic nematic LC cell:

$$I_{th_nematic} = \frac{\pi^2 K_{33} c n_e^2}{(n_e^2 - n_o^2) n_o d^2}, \quad (5)$$

Similar to the case of realignment by low-frequency electric fields, the twisting tendency of the CLC augments the action of the electric field at an optical frequency so that the director realignment can be observed at lower laser intensities. Furthermore, by changing ρ , one can obtain the director reorientation at low (~ 10 -50 mW) threshold laser intensities and applied voltages. Since $w \approx d$ in most of our experiments and the assumption $w \gg d$ does not hold, the above expressions describe the switching behavior only qualitatively.

Initial stages of the director realignment in homeotropic CLC cells [Fig. 1(b)] at laser intensities around I_{th} are qualitatively similar to those in nematic cells [23–26]. However, the dynamic evolution of $\hat{n}(\vec{r})$ at higher intensities differs substantially and a broad range of 3D twisted configurations can be formed. Furthermore, above well-defined 2nd threshold laser intensity I_{th2} , one can obtain multistable localized configurations that do not disappear upon switching off the beam. Because of the 3D twisted nature of the involved $\hat{n}(\vec{r})$, numerical approaches need to be utilized in order to obtain insights into the kinetics of the evolution of $\hat{n}(\vec{r})$ and the dependence of I_{th2} on the CLC cell and material parameters [14].

4. Experimental results

In our experiments, the LC is confined between two glass plates treated to align $\hat{n}(\vec{r})$ vertically. These boundary conditions are incompatible with the uniform one-directional twist of the equilibrium cholesteric structure, causing the frustrated unwound director structure, Fig. 1(a). When a laser beam with the intensity slightly above the realignment threshold value I_{th} (typically 1-10 MW/cm², depending on cell thickness and pitch) is focused into the bulk of the unwound CLC, the beam rotates $\hat{n}(\vec{r})$ toward the lateral $\vec{E}(\vec{r}) \perp \hat{z}$. The ensuing $\hat{n}(\vec{r})$ minimizes the free energy term describing the coupling of the director and optical-frequency electric field of the beam, Eq. (2). Due to the positive dielectric anisotropy of CLC for the light's electric field $\vec{E}(\vec{r})$, the laser beam produces a structure with lateral $\hat{n}(\vec{r})$ along the beam's linear polarization direction, Fig. 1(b). This initial distortion (birefringent spot observed in polarized optical microscopy textures such as the one shown in Fig. 1(c)) is usually obtained at an average power above a threshold value $P_{th} = (30$ -50) mW when a diameter of focal spot is about 1 μ m and disappears within 5-10 ms after turning off the laser or shifting the laser beam to a different location. This "self-healing" of the distorted structure takes place in order to minimize the elastic energy given by Eq. (1) at no applied field.

In addition to the optical-frequency control by laser beams, the cholesteric structures can be further controlled electrically. In the case of CLCs with positive low-frequency dielectric anisotropy $\Delta\epsilon_{lf} > 0$, the applied voltage facilitates disappearance of the director distortions as the vertical low-frequency electric field opposes the action of the optical-frequency electric field of the laser. In contrast, for CLC materials with $\Delta\epsilon_{lf} < 0$, the action of applied voltage augments that of the focused laser beam, lowering the threshold laser beam intensity needed to induce these distortions, since the vertical low-frequency electric field stabilizes the in-plane alignment of the director. We observe that if the laser intensity is increased above the second threshold $I_{th2} = (1.2$ -2.2) $\cdot I_{th}$, the initial laser-induced director distortions transform into

localized triple-twisted structures persisting even after the laser is switched off [Fig. 1(d)] [14]. These localized structures are embedded in a sea of uniform director field and have a characteristic size $\approx p$ in all directions. By controlling the laser beam's intensity and voltages applied to CLCs with positive or negative dielectric anisotropy, one can generate arbitrary patterns consisting of multiple localized laser-induced structures controlled dynamically by computer-programmed laser intensity distributions.

Polarization-sensitive nonlinear optical 3D imaging [20–22] reveals that the localized cholesteric structures generated by Gaussian beams are the so-called triple twist Torons of the first kind (T3-1) (Fig. 2) [14]. Such structures can spontaneously occur in CLCs confined into homeotropic cells, similar to the so-called cholesteric fingers and cholesteric bubbles [12, 13, 27–33]. In the reconstructed director field configuration (Fig. 2), one can distinguish the disclination ring of a “twist-escaped” disclination of strength “+1” with non-singular core and two point defects of topological charge “-1” nearby the opposite confined surfaces (shown by the red dots in Fig. 2(b)), characteristic of the T3-1 [14].

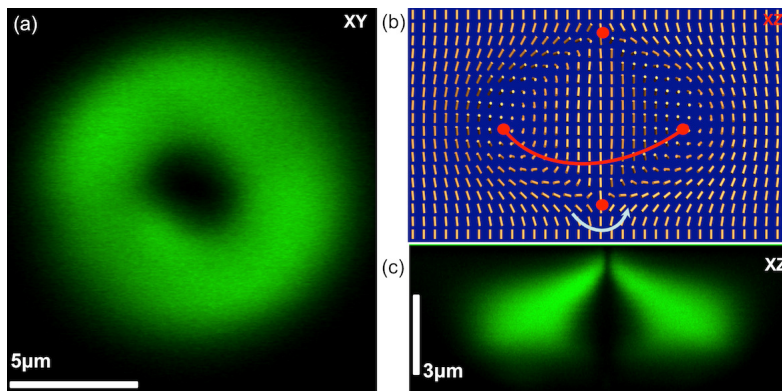


Fig. 2. 3PEF-PM imaging of laser-generated director structures. (a) In-plane 3PEF-PM image obtained for circular polarization of excitation light. (b) Reconstructed director field in the vertical cross-section of the axially symmetric Toron and (c) the corresponding vertical cross-section 3PEF-PM image obtained for the circular polarization of excitation laser light.

Robust optical generation and subsequent manipulation of arbitrary structures composed of localized multistable particle-like excitations may enable a broad range of photonic and electro-optic applications such as optically-reconfigurable diffraction gratings. We have achieved generation of periodic patterns composed of the Torons by a scanning laser beam and also by utilizing laser intensity distributions from holograms generated by the SLM. Examples of holographically-generated structures include the one comprising characters “LCMRC” (stands for the Liquid Crystal Materials Research Center) [Fig. 3(a)], a periodic square lattice with a deliberately-introduced dislocation defect [Fig. 3(b)] that can be seen from the reconstructed Voronoi diagram in Fig. 3(c), and a spiraling pattern of Torons [Fig. 3(d)] with the respective Voronoi diagram shown in Fig. 3(e).

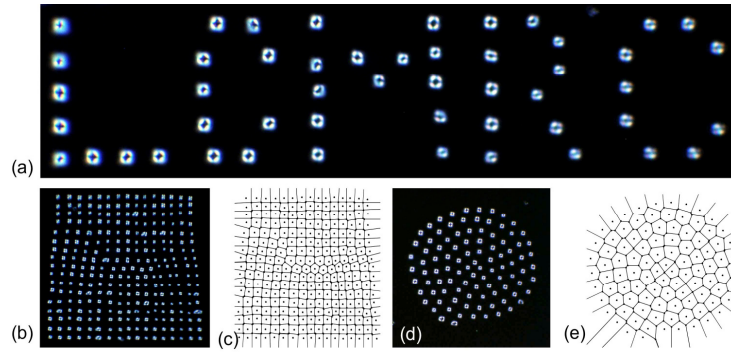


Fig. 3. Polarized optical micrographs of laser-induced patterns of Torons generated using HOLCAS. (a) A pattern forming the letters 'LCMRC'. (b) Square-periodic 2D array of Torons with a deliberately introduced dislocation in the center and (c) the corresponding Voronoi construction; the image in (a) is 250 μm in width. (d) A 2D spiraling pattern of Torons and (e) the corresponding Voronoi diagram. The lateral size of Torons in (b) and (d) is 5 μm .

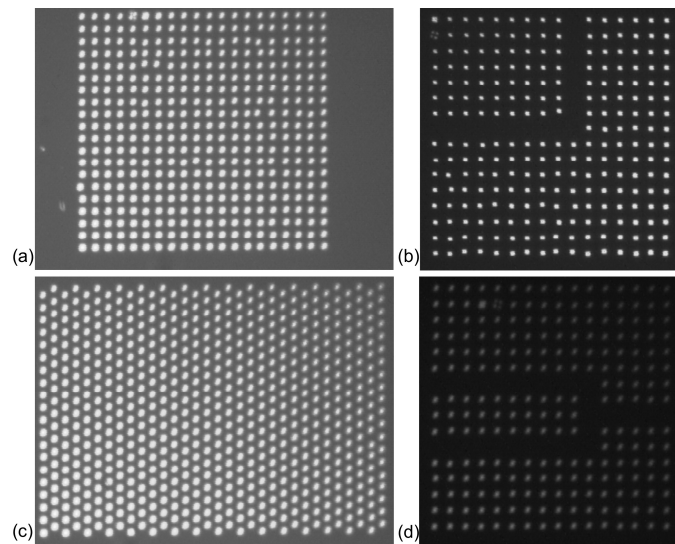


Fig. 4. Polarized optical micrographs showing photonic structures of Torons generated using the laser beam scanning approach. (a) Sequentially-generated 20x20 square array of Torons (Media 3); the image is 280 μm in width. (b) Square-periodic pattern of Torons having an L-shaped channel with vertical $\hat{n}(\vec{r})$ (Media 4); the image width is 320 μm . (c) Sequential generation of a hexagonal array of Torons (Media 5); the image width is 330 μm . (d) A square-periodic array of Torons with a bifurcated channel (Media 6); the image width is 320 μm . The micrographs were obtained using two crossed polarizers oriented along vertical and horizontal edges.

In the scanned-beam approach, the focused laser beam is steered within the sample following computer-programmed patterns and generates programmed superstructures with well-defined positions of Torons that can be further reconfigured by using optical manipulation, erased by applying voltage (for materials with positive low-frequency dielectric anisotropy), as well as dynamically controlled by a combination of these means (Fig. 4). Examples of laser-generated structures include square-periodic [Fig. 4(a)] and hexagonal [Fig. 4(c)] crystalline arrays of Torons, as well as periodic arrays with deliberately introduced channel-like defects in the translational order [Fig. 4(b) and 4(d)]. Figure 5 shows that complex electrically-switchable periodic super-lattices can be obtained by sequential generation of the Torons in a homeotropic cell [Fig. 5(a)] by first producing a square-periodic

pattern of sparsely spaced Torons [Fig. 5(b)] and then introducing a new array of Torons in locations in-between the Torons of the initial square lattice [Fig. 5(c) and 5(d)].

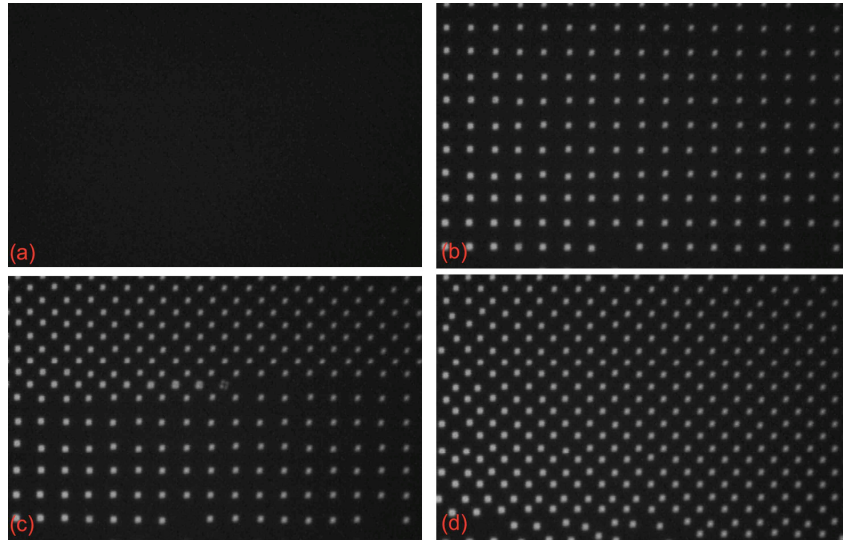


Fig. 5. Sequentially generated square-periodic pattern obtained by laser beam scanning method. In a cell with (a) initial homeotropic alignment of $\hat{n}(\vec{r})$, the scanned beam first generates (b) a square-periodic pattern of sparsely spaced Torons with a larger periodicity and then (c) additional Torons are introduced in-between the Torons of the original square array so that (d) the final translationally periodic pattern of Torons has a smaller periodicity. (Media 7) The optical micrographs have 320 μm in width and were obtained between two crossed polarizers oriented along the vertical and horizontal image edges.

The lateral size of Torons and the minimum spatial periodicity of the laser-induced photonic crystal structures can be adjusted by using CLC materials of different pitch. Since the minimum size of the optically-generated Toron structures is close to the equilibrium pitch p [14], in principle, the periodicity of the photonic lattices can be made comparable to the wavelength of light in the visible spectral range and controlled (by varying p and cell thickness d while keeping $p/d \approx 1$) in the range from 200 nm to hundreds of microns. In addition to the laser beams, control over the director structures can be achieved by using a low-frequency electric field applied to the patterned transparent electrodes at the confining substrates.

An important property of the studied cholesteric cells is that they can host different uniform and twisted 3D structures of $\hat{n}(\vec{r})$ that can be switched between each other both optically and electrically (Fig. 6). CLCs in homeotropic cells with $p/d \approx 1$ can have a stable uniform state with the director orthogonal to the cell bounding plates [Fig. 6(a)]. The laser generated localized Torons can be transformed into a uniform unwound state by applying electric field (if low-frequency dielectric anisotropy is positive) to the transparent ITO electrodes or optically by using laser intensity distributions incompatible with the existing Toron structures (Fig. 6). Importantly, both uniform unwound and localized twisted states can be stable for long time, since the spontaneous transformation between these director configurations requires nucleation of additional topological defects that define strong energy barriers. Elastic-energy density in the sample regions with unwound $\hat{n}(\vec{r})$ surrounding the Torons has minimum splay and bend contributions described by the first and third terms in Eq. (1). However, these regions have relatively large twist energy density (second term) and saddle splay energy described by the fourth term in Eq. (1). Torons locally minimize the twist and saddle-splay terms at the expense of enhancing the splay and bend distortions and

introducing point defects [Fig. 2(b)]. This enables both electrical and optical multistable local switching between the unwound state and a Toron (Fig. 6).

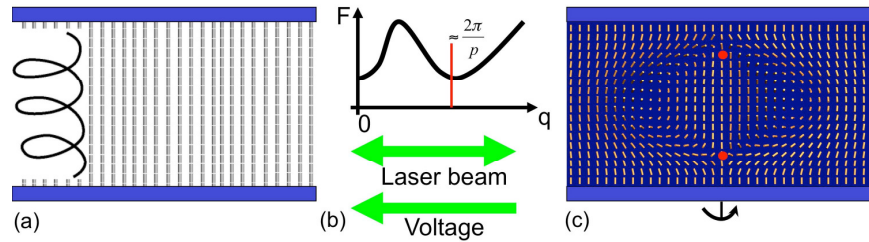


Fig. 6. Schematics of switching between a uniform unwound and 3D localized twisted configurations. (a) Cholesteric LC with the tendency to twist (shown by the spiral in the inset) is unwound via confinement into a cell with strong vertical surface boundary conditions. (b) Schematic illustration of elastic free energy dependence on $q = 2\pi/p$ showing two local/global minima corresponding to the unwound state shown in (a) and 3D twisted state of the Toron structure shown in (c). The cell can be switched between the unwound state shown in (a) and the 3D twisted state shown in (c) by laser beam helping to overcome the elastic energy barrier separating the two distinct states. For LC materials with positive $\Delta\epsilon_{if}$, the localized structure shown in (c) can be unwound and transformed to the uniform $\hat{n}(\vec{r})$ shown in (a) by voltage applied to the transparent electrodes at confining plates, as marked by the green arrow in (b).

Additional control over the optically induced CLC structures can be obtained via continuous scanning of the focused laser beam at varying speeds. Very slow scanning with speeds below or about $1 \mu\text{m/s}$ simply results in optical manipulation of the position of the Toron generated by a focused laser beam. Figure 7 shows that the increase of the speed of continuous scanning causes stretching of Torons [Fig. 7(a)] and their merging into various linear defect structures [Fig. 7(b)-7(d)], as well as generation of these linear defect structures in a homeotropic cell environment with no Torons initially present (Fig. 1). We have identified these linear defect structures as cholesteric fingers, which, similar to Torons, contain regions with local 3D director twist [12, 13]. These linear defect structures are stable after switching off the laser; this stability has the same physical underpinnings as that of Torons (Fig. 7). The video linked to Fig. 7(e) (Media 11) demonstrates that, similar to the case of Torons, these linear cholesteric structures can also be “erased” by applying low-voltage electric fields and then generated repeatedly. Thus, in homeotropic cholesteric cells with $p \approx d$, in addition to the unwound uniform homeotropic structure, one can locally induce fingers and Torons that can be spatially patterned at will.

In the studied CLC cells, the local effective refractive index n_{eff} varies within a value range between the ordinary n_o and extraordinary n_e indices, depending on the light propagation direction with respect to $\hat{n}(\vec{r})$. For light incident orthogonally to the LC cell, the local effective index is $n_{eff} = n_o$ in the areas with uniform vertical director. Within the localized Toron structures [Fig. 2(f)], the effective refractive index depends on the orientation of $\hat{n}(\vec{r})$ with respect to the light polarization direction. For linearly polarized light propagating as an extraordinary wave, the effective refractive index is $n_{eff} = n_o n_e / (n_e^2 \cos^2 \theta + n_o^2 \sin^2 \theta)^{1/2}$, where θ is the angle between the light propagation direction and $\hat{n}(\vec{r})$. This results in a refractive index contrast between the Toron domains and the surrounding homeotropic texture, being dependent on the direction of light propagation and the light polarization direction. In periodic laser-generated structures (Figs. 2-5), LC domains of higher and lower effective refracting index produce ordered photonic structures. Although the values of optical anisotropy of LCs are typically smaller than 0.5, nevertheless, photonic applications that do not require a large refractive index contrast providing the full photonic band gap (such as lasing [6–8] and diffraction gratings) can be potentially realized.

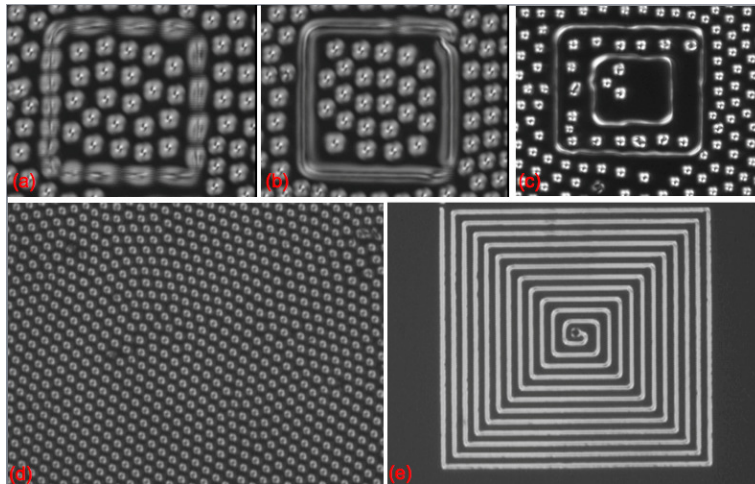


Fig. 7. Generation of cholesteric fingers via continuous scanning of a focused laser beam. (a) Scanning of the laser beam along a perimeter of a rectangle causes a complex dynamics and slight stretching of Torons along the direction of beam scanning (Media 8). (b) Merging of Torons along the direction of laser beam scanning to form the linear structures of cholesteric fingers (Media 9). (c) Director structures comprising Torons and fingers obtained by means of computer-programmed laser scanning. (d) Generation of linear defect structures via merging of Torons (Media 10). (e) The linear defect structures can be also generated via continuous slow scanning of a focused beam in a homeotropic cell (Media 11). The lateral size of Torons and fingers in (a-e) is 5 μm .

5. Conclusion

We have demonstrated optical generation of arbitrary two-dimensional photonic patterns composed of localized cholesteric particle-like structures. These laser-generated photonic assemblies can be dynamically controlled and reconfigured using light and electric fields. They have potential uses for applications in all-optical light manipulation in diffractive optics, telecommunication, optoelectronics, optical computer integrated systems, tunable dispersion materials, tunable gratings in multiplex system, adaptive optics, all-optical information displays, optical data storage, and other all-optical photonic devices. Laser control of cholesteric structures can be extended to other stable and metastable structures such as cholesteric fingers, Torons of other types, cholesteric bubbles, umbilical and other textures [12–14,27–33].

Acknowledgments

This work was supported by the Institute for Complex Adaptive Matter (IIS, CWT), the Directorate of Chemistry and Life Sciences of Air Force Office of Scientific Research (DK, AVK, ANK, PNP), and NSF grants nos. DMR-0820579 (IIS, TL, RPT) and DMR-0847782 (IIS, PJA). We acknowledge discussions with N.A. Clark, D. Gardner, Y. Lansac, and B.I. Senyuk.